nature ecology & evolution

Article

https://doi.org/10.1038/s41559-025-02806-4

Lagged precipitation effects on plant production across terrestrial biomes

Received: 25 November 2024

Accepted: 23 June 2025

Published online: 28 July 2025

Check for updates

Lei He[1], Jian Wang[2,3] ✉, Drew M. P. Peltier[4], François Ritter[5], Philippe Ciais[5], Josep Peñuelas[6,7], Jingfeng Xiao[8], Thomas W. Crowther[9], Xing Li[10], Jian-Sheng Ye[11], Takehiro Sasaki[12], Chenghu Zhou[13] & Zhao-Liang Li[1,14] ✉

Precipitation effects on plant carbon uptake extend beyond immediate timeframes, reflecting temporal lags between rainfall and plant growth. Mechanisms and relative importance of such lagged effects are expected to vary across ecosystems. Here we draw on an extensive collections of productivity proxies from long-term ground measurements, satellite observations and model simulations to show that preceding-year precipitation exerts a comparable influence on plant productivity to current-year precipitation. Statistically supported lagged precipitation effects are detected in 13.4%–19.7% of the grids depending on the data source. In these sites, preceding-year precipitation positively controls current-year plant productivity in water-limited areas, while negative effects occur in some wet regions, such as tropical forests. While aridity emerges as the main driver of this spatial variability, machine learning-based spatial attribution also indicates interactions among plant traits, climatic conditions and soil properties. We also show that soil water dynamics, plant phenology and foliar structure might mediate lagged precipitation effects across time. Our findings highlight the role of preceding-year precipitation in global plant productivity.

Precipitation is the major constraint on soil water availability and plant growth, thereby affecting ecosystem structure and functioning and fluxes of energy and carbon[1–3]. As such, plants have greater productivity in wet than in dry regions, highlighting an emergent control of precipitation on plant productivity from a spatial perspective[4]. However, concurrent precipitation explains a fairly limited amount of plant productivity at a given site or region, because precipitation impacts may linger in time[5–7]. Lagged precipitation effects (LPEs), the delayed impacts of antecedent precipitation, may be a central driver of sustained plant productivity[8,9]. As precipitation becomes both more extreme and variable under warming[10,11], recognizing and improving our understanding of LPEs is critical for ecological and agricultural practices[12,13] and ecosystem functioning and carbon cycling[5,14].

Previous studies have highlighted the lingering effects of past drought events on plant productivity, commonly referred to as 'drought legacies'[5,15–18]. In contrast, LPEs capture the influence of antecedent precipitation over annual to multiyear timescales, irrespective of whether those periods include extreme events and reflect a form of precipitation 'memory' effect[17]. However, identifying and elucidating this precipitation memory effect (that is, LPEs) has proved challenging[19]. Empirical efforts, relying on manipulative experiments or site-level observations, have yielded inconsistent results due to discrepancies in productivity proxies, spatial scale, ecological context and quantitative apporoches[8,14,15,20], thereby complicating attempts to discern overarching patterns and general mechanisms. A leading hypothesis attributes LPEs to plant physiological memory, wherein resources such as carbohydrates and nitrogen are stored in specific organs during favourable periods and later remobilized to support growth or reproduction under stress[17,21,22]. Accordingly, positive LPEs have been widely documented in semi-arid grasslands[7,9,23], savanna ecosystems[24]

A full list of affiliations appears at the end of the paper. ✉e-mail: wangjian@igsnrr.ac.cn; lizhaoliang@caas.cn

https://doi.org/10.1038/s41559-025-02806-4

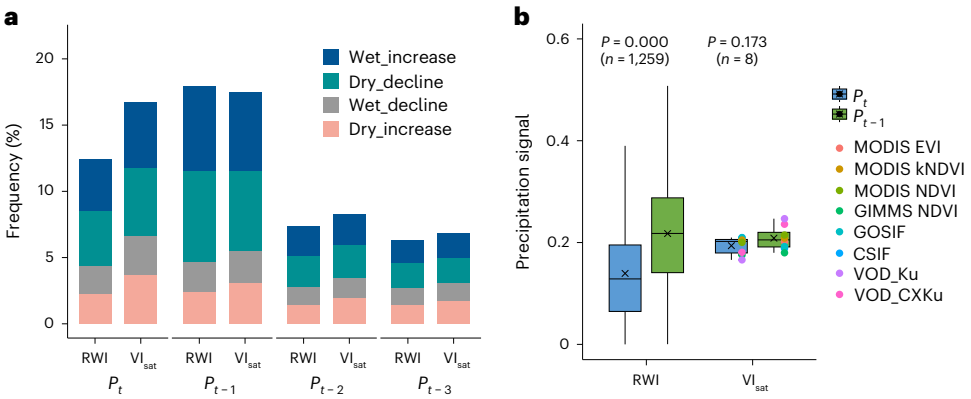

Fig. 1 | Comparison of effects of current-year and antecedent precipitation on plant productivity. a, Frequencies of sites (RWI, $n = 4{,}852$) and grids (VI_{sat}) with significant partial correlations ($P < 0.05$) between plant productivity and precipitation for the current year (P_t), with 1-yr (P_{t-1}), 2-yr (P_{t-2}) and 3-yr (P_{t-3}) lags. The VI_{sat}-based results were determined as the mean frequency of eight VI_{sat} datasets. A two-sided Student's *t*-test showed no significant difference in frequency between P_t and P_{t-1} among VI_{sat} datasets ($P = 0.758$, $n = 8$). Sites or grids with significant partial correlations were categorized into four groups on the basis of anomalies in precipitation and productivity: 'wet' and 'dry' represent positive and negative precipitation anomalies, respectively; and 'increase' and 'decline' correspond to positive and negative productivity anomalies, respectively. **b**, Distribution of precipitation signals (absolute values of ridge-regression coefficients, unitless) for the current year (P_t) and the preceding year (P_{t-1}). Sites or grids were included if plant productivity was significantly sensitive to precipitation in either the current or preceding year. Precipitation signals were compared across RWI sites ($n = 1{,}259$) and among VI_{sat} datasets ($n = 8$). Boxplots show the mean (cross), median (line), 25th–75th percentiles (box) and whiskers to the minimum and maximum within 1.5× the interquartile range (75th minus 25th percentile) from the box edges. *P* values reflect significance levels based on two-sided Student's *t*-tests.

and temperate forests[25], where higher precipitation in preceding years enhances soil moisture storage, plant growth (for example, increases in leaf area and sapwood area) and nutrient mineralization, subsequently boosting plant productivity in the current year.

Conversely, negative LPEs—whereby higher antecedent precipitation reduces subsequent productivity—have been less frequently reported but may emerge in extreme wet regions (for example, >3,000 mm yr^{-1}), such as tropical rainforests[26]. These negative responses are potentially driven by chronic soil waterlogging[27,28], nutrient leaching[29] and indirect structural shifts in canopy composition or light availability[6]. Similarly, reduced precipitation or brief droughts accompanied by increased solar radiation may enhance concurrent or near-future photosynthetic capacity in rainforest canopies[30,31]. These contrasting LPE patterns highlight biome-specific trade-offs in water–energy balance and reflect the diverse acclimation and adaptation strategies used by vegetation in response to climatic variability[6,8,9].

Yet, in contrast to the extensively studied drought legacies, the direction and magnitude of LPEs remain poorly understood, and have not been characterized at global scales. Underlying mechanisms are also likely to differ across ecosystems (forests and grasslands) and across time, limiting our ability to predict vegetation productivity under shifting precipitation regimes. To address this, we developed an integrated framework to assess LPEs on plant productivity across spatial scales, combining precipitation records with long-term productivity metrics or proxies derived from ground observations, satellite remote sensing and model outputs. We systematically quantified the direction and magnitude of LPEs from site to global scales and used machine learning-based spatial attribution analysis to disentangle the contributions of biotic and abiotic drivers to their geographic variability. Furthermore, we investigated the temporal mechanisms underpinning LPEs, focusing on the mediating roles of soil moisture dynamics, leaf structural traits and phenological responses.

Results

Comparison of preceding-year versus current-year precipitation effects on plant productivity

We analysed long-term ground-based monitoring data of tree-ring-width index (RWI), a proxy for annual tree productivity (Supplementary Fig. 1), alongside eight satellite-derived vegetation indices (VI_{sat}) (Supplementary Table 1), to assess the effects of preceding-year versus current-year precipitation on plant productivity. Partial correlation analyses were conducted to isolate the effects of precipitation from preceding years (up to a 3-yr lag) and the current year, while controlling for precipitation during other periods and additional climatic factors, including annual mean near-surface temperature and total surface downwelling solar radiation. Our results showed that 12.4% of RWI sites exhibited significant partial correlations with current-year precipitation, aligning with VI_{sat}-based analysis, which showed 16.7 ± 1.1% (mean ± s.e.) of grids with significant partial correlations ($P < 0.05$). Preceding-year precipitation (1-yr lag) had a comparable influence on productivity to current-year precipitation, as evidenced by a higher frequency of significant partial correlations (17.9% for RWI sites and 17.5 ± 2.1% for VI_{sat} pixels), while the effects of precipitation with 2- and 3-yr lags were notably weaker. We further categorized sites and grids with significant correlations into four groups on the basis of anomalies in precipitation and productivity proxies (Methods). Positive correlations—where wet (dry) years were followed by increases (declines) in productivity—were substantially more frequent than negative correlations, where wet (dry) years preceded productivity declines (increases) (Fig. 1a). These results underscore the widespread positive effects of precipitation across different time lags on plant productivity.

To quantify the magnitude of precipitation effects, we applied ridge regression to address potential collinearity among drivers (Methods). Our results showed that the precipitation signals (defined as the absolute value of regression coefficients) from the preceding year were similar or higher than those from the current year (RWI $P < 0.001$; VI_{sat} $P = 0.173$) (Fig. 1b). Approximately 10% of the variance in RWI- and VI_{sat}-based metrics was attributed to preceding-year precipitation, close to or exceeding the variance explained by current-year precipitation (RWI $P < 0.001$; VI_{sat} $P = 0.495$) (Supplementary Fig. 2). Biome-level- and growing-season-based analyses further demonstrated that the influence of preceding-year precipitation on plant productivity was comparable to that of current-year precipitation (Supplementary Figs. 3–6), highlighting the important role of antecedent precipitation across scales. To examine the effects of climate extremes, we conducted the same analyses after removing abnormal years with 1, 1.5 and 2 s.d., and found overall consistent results (Supplementary Fig. 7).

https://doi.org/10.1038/s41559-025-02806-4

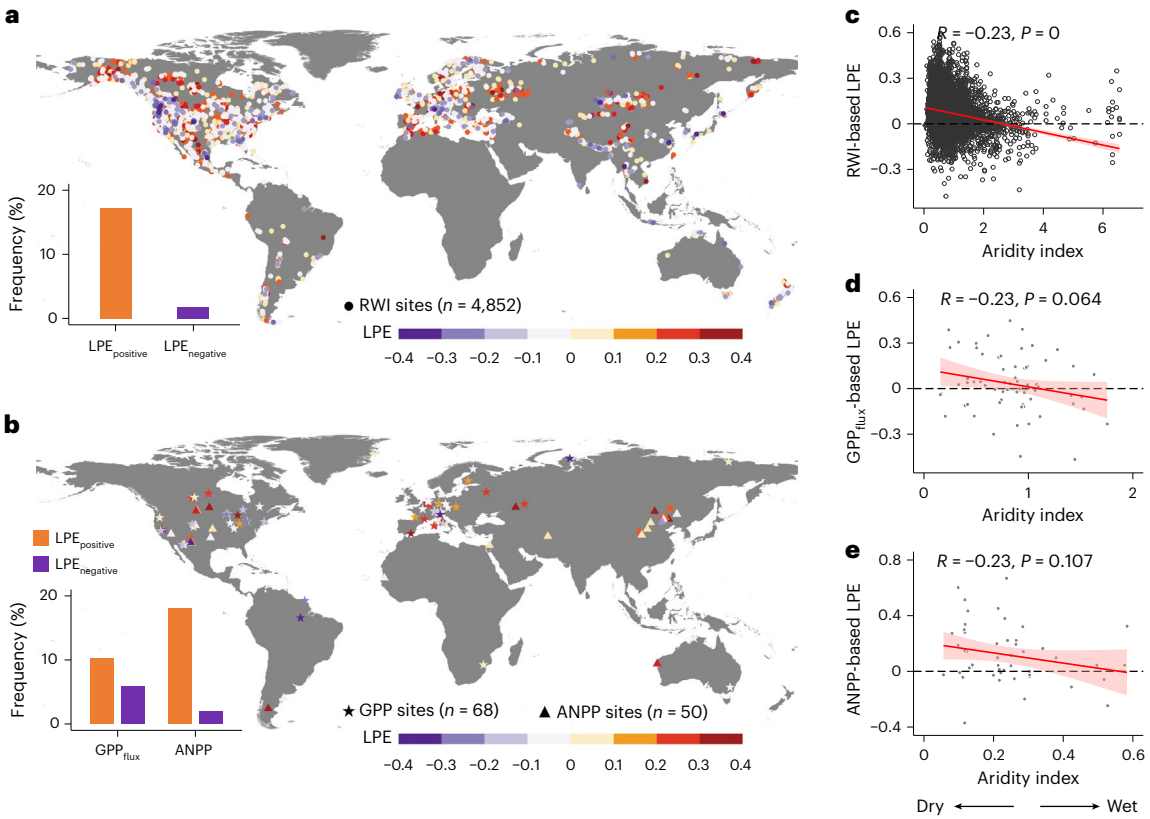

Fig. 2 | LPEs on plant productivity inferred from ground-based measurements. **a**, LPE patterns for RWI. **b**, LPE patterns for GPP_{flux} and grass ANPP. $LPE_{positive}$ and $LPE_{negative}$ indicate positive and negative LPE, respectively. **c**–**e**, Relationships between aridity index (precipitation-to-potential evapotranspiration ratio) and LPEs for RWI (**c**), GPP_{flux} (**d**) and ANPP (**e**). In **c**–**e**, red lines show the fitted values from the ordinary least squares regression, with red shading representing the 95% confidence intervals. *R* indicates the correlation coefficient between LPE and the aridity index and *P* values are derived from two-sided *t*-tests of the regression coefficients.

Additionally, we examined the role of preceding-year precipitation in regulating concurrent productivity, using a nonlinear regression method (generalized additive models, GAMs) (Supplementary Fig. 8) and substituting precipitation data with the standardized precipitation evapotranspiration index (SPEI) (Supplementary Fig. 9). Collectively, these analyses consistently confirmed the substantial effects of preceding-year precipitation on plant productivity variability.

LPEs on plant productivity from site to global scales

Given the notable influence of preceding-year precipitation on plant productivity, we quantified LPEs using ridge-regression-based sensitivity analyses across multiscale productivity proxies (Methods). We assessed site-level LPEs using three independent ground-based productivity proxies: (1) RWI, (2) eddy-covariance flux-derived gross primary productivity (GPP_{flux}) and (3) grass aboveground net primary production (ANPP) (Supplementary Figs. 1, 10 and 11). RWI data from 4,852 sites identified LPEs at 19.0% of the sites, with 17.2% showing positive and 1.8% showing negative LPEs (Fig. 2a). Classification of sites by tree type (angiosperms and gymnosperms) confirmed a predominance of positive LPEs, with angiosperm sites showing comparable LPEs to those of gymnosperm sites (Supplementary Fig. 12). Grassland ANPP data from 50 sites revealed similar patterns, with 18.0% and 2.0% of sites exhibiting positive and negative LPEs, respectively. The GPP_{flux} data (68 sites) indicated a weaker prevalence of positive LPEs, with 10.3% showing positive and 5.9% showing negative LPEs (Fig. 2b). We observed consistently negative correlations between the aridity index (precipitation/potential evapotranspiration ratio, with lower values indicating more arid conditions) and LPEs across all three datasets, with positive LPEs tending to occur in arid regions and negative LPEs in wetter regions (Fig. 2c–e), highlighting the aridity-dependent nature of LPEs as derived from ground-based measurements.

Consistent with findings from ground-based networks, global-scale analyses using eight VI_{sat}, eight satellite-derived estimates of GPP (GPP_{sat}) and 18 GPP simulations from carbon-cycle models (GPP_{model}) (Supplementary Tables 1 and 2) confirmed the widespread occurrence of LPEs, with a notable predominance of positive LPEs (Fig. 3). Specifically, analyses of eight VI_{sat} metrics revealed widespread positive LPEs (16.9%) mainly in arid and semi-arid regions, whereas negative LPEs (2.8%) were more prevalent in humid regions, such as tropical forests in South America and central Africa, as well as mid-to-high latitude Europe (Fig. 3a). The aridity-dependent nature of VI_{sat}-based LPEs was further supported by significant negative correlations between LPEs and the aridity index ($P < 0.001$) (Fig. 3b). Among VI_{sat} metrics, we found similar magnitudes and spatial patterns of LPEs (Supplementary Figs. 13 and 14), while results from satellite-derived vegetation optical depth (VOD), a proxy of vegetation biomass and water content, exhibited higher magnitudes and more evident patterns of LPEs than other VI_{sat} metrics. Similar spatial patterns and aridity dependencies were observed in GPP_{sat}-based analyses with eight datasets, although the proportions and magnitudes differed (positive LPE 11.4%; negative LPE 2.0%) (Fig. 3c,d and Supplementary Fig. 15). Using GPP_{model} (Supplementary Table 2), we also identified widespread positive LPEs (12.5%) and significant negative correlations between LPEs and the aridity index (Fig. 3e,f). However, the consistency of LPE patterns across models was limited, as indicated by divergent spatial patterns of LPEs and relatively high standard deviations across models compared with VI_{sat} and GPP_{sat} metrics (Supplementary Figs. 16 and 17). Collectively, evidence from diverse datasets confirms

https://doi.org/10.1038/s41559-025-02806-4

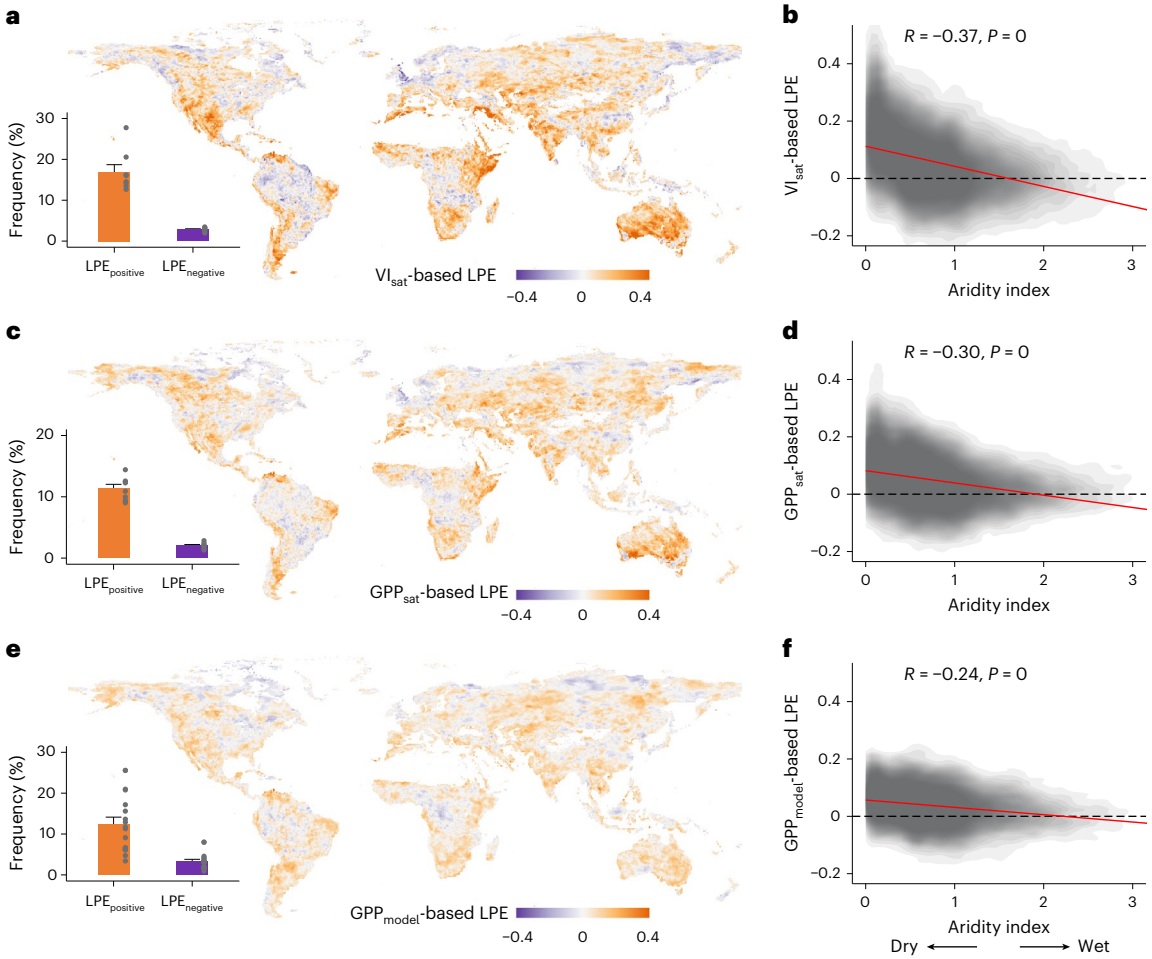

Fig. 3 | LPEs on plant productivity inferred from satellite observations and model simulations. a,**c**,**e**, Spatial patterns of LPEs for VI_{sat} (**a**), GPP_{sat} (**c**) and GPP_{model} (**e**). For each grid, the map values represent the mean LPEs from collections of VI_{sat} ($n = 8$), GPP_{sat} ($n = 8$) and GPP_{model} ($n = 18$). In inner subplots, error bars indicate half the standard error and grey points indicate the frequency (%) of significant LPE grids for each dataset. Spatial distributions of LPEs for individual datasets and standard deviations in LPEs are provided in Supplementary Figs. 13–17. **b**,**d**,**f**, Relationships between aridity index (precipitation-to-potential evapotranspiration ratio) and LPEs for VI_{sat} (**b**), GPP_{sat} (**d**) and GPP_{model} (**f**). In **b**,**d** and **f**, red lines show the fitted values from the ordinary least squares regression. *R* indicates the correlation coefficient between LPE and the aridity index and *P* values are derived from two-sided *t*-tests of the regression coefficients.

the global, aridity-dependent patterns of LPEs. However, compared with VI_{sat}-based analyses, the magnitudes of LPEs and the frequencies of positive LPEs from GPP_{sat}- and GPP_{model}-based analyses were generally lower.

Potential mechanisms underlying LPEs

We evaluated the relative contributions of biotic and abiotic factors to the spatial variability of LPEs using a random forest (RF) model coupled with Shapley additive explanations (SHAP) analysis (Methods). In the grid-based (VI_{sat}) analysis, the RF model explained 71% of spatial variability in LPEs ($R^2 = 0.71 \pm 0.05$). Among the factors, the aridity index was the most influential, showing a negative correlation with LPEs. Consistently, areas characterized by high radiation or low precipitation predominantly exhibited positive LPEs (Fig. 4a). Additionally, regions with lower soil pH (more acidic soils) tended to exhibit negative LPEs (Supplementary Fig. 18). Although RF models explained a smaller proportion of site-level LPE variability ($R^2 = 0.34$), we observed similar climatic, vegetation and soil controls in RWI-based analyses. Climatic variables, particularly the aridity index, were the dominant drivers of spatial variability in LPEs (Fig. 4b). Notably, grids or sites with lower plant species richness or greater variance in productivity proxies tended to exhibit stronger LPEs (Fig. 4a,b and Supplementary Fig. 19), suggesting that ecosystem structure and resilience mediate the spatial patterns of LPEs.

From a temporal perspective, we tested three hypotheses to explain the divergent LPEs as follows. H1 (background moisture condition): increases in preceding-year precipitation may enhance soil moisture storage and availability (and/or snowpack), thereby boosting plant productivity in water-limited regions (positive LPE)[32]. However, excessive precipitation in the past may lead to soil oversaturation in water-sufficient areas, reducing aeration and causing waterlogging, which inhibits photosynthetic activity (negative LPE)[27,28]. H2 (biological carryover effect): larger leaf area is associated with a greater capacity for carbon uptake. However, preceding-year precipitation may have contrasting effects on leaf area due to the balance between water and energy limitations. These shifts in leaf structure could carry over into the following year, influencing plant productivity. We note that leaf area shifts may be reflective of other physiological changes that are harder to observe, but may also drive LPEs, such as changes in sapwood conducting area, rooting area or carbohydrate reserves[9,33]. H3 (phenological control): preceding-year precipitation may impact green-up date, a key determinant of growing-season length for the subsequent year, thereby affecting plant productivity in different directions[34]. To test these hypotheses, we applied partial correlation analyses and

https://doi.org/10.1038/s41559-025-02806-4

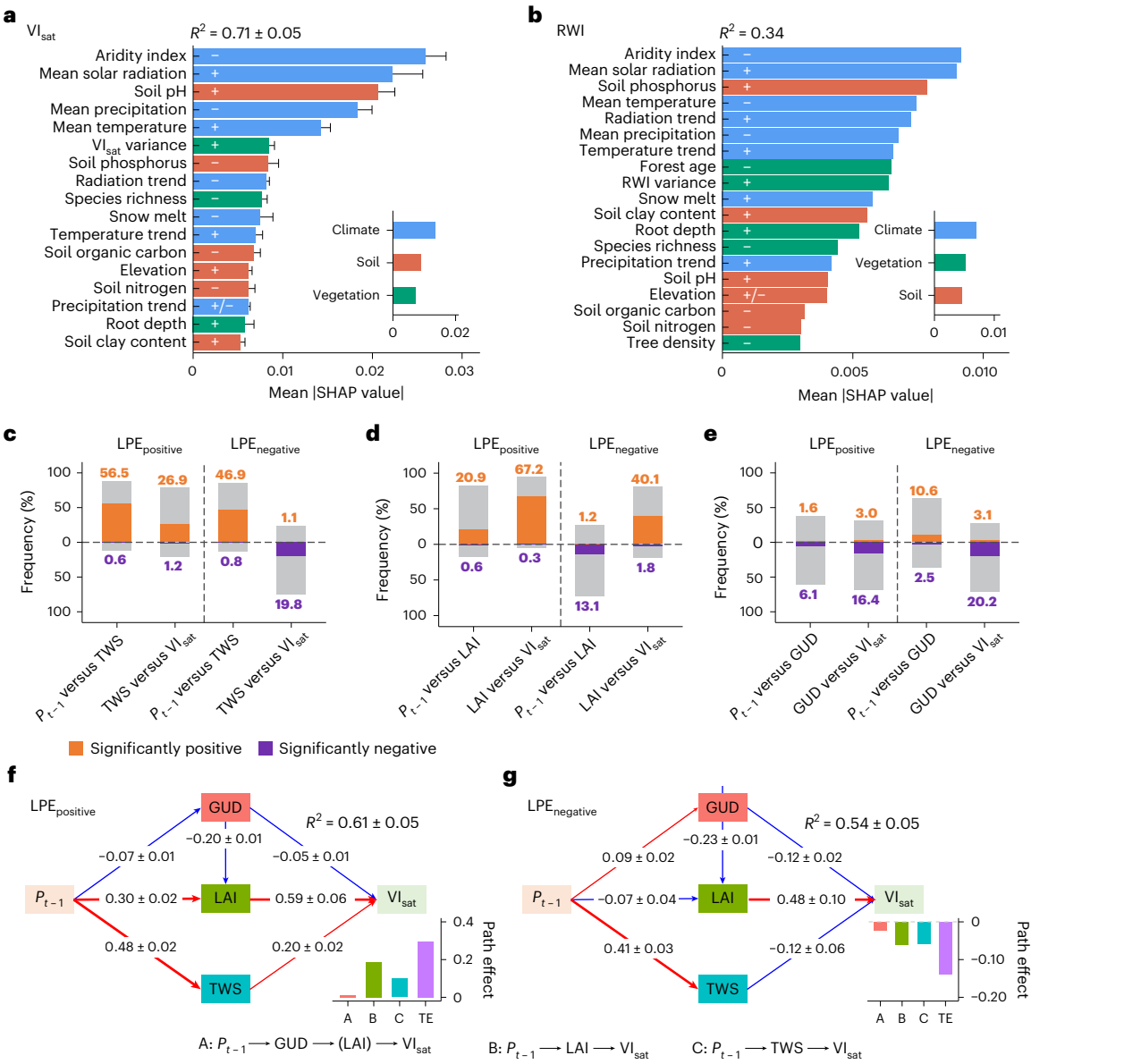

Fig. 4 | Spatial attribution and temporal mechanisms of LPEs. a,**b**, Relative importance of biotic and abiotic factors controlling the spatial variability of VI_{sat}-based LPEs (**a**) ($R^2 = 0.71 \pm 0.05$, $n = 8$) and RWI-based LPEs (**b**) ($R^2 = 0.34$), as determined by RF models using mean absolute SHAP values. In **a**, error bars indicate the standard error across VI_{sat} datasets. The symbols '+' and '−' indicate significantly positive and negative relationships between LPE and predictors ($P < 0.05$), respectively, with at least five VI_{sat} metrics showing consistent results in **a**. The symbol '±' indicates no significant relationship. The inner subplot indicates the averaged importance of climate, vegetation and soil factors. **c**–**e**, Distributions of partial correlation coefficients for three mediators: relationships include preceding-year precipitation (P_{t-1}) versus current-year TWS and TWS versus satellite-observed vegetation indices (VI_{sat}) (**c**); P_{t-1} versus LAI and LAI versus VI_{sat} (**d**); and P_{t-1} versus GUD and GUD versus VI_{sat} (**e**). Statistical significance was set at $P < 0.05$. **f**,**g**, SEMs describing the positive (**f**) and negative (**g**) LPEs incorporating the effects of mediators. Numbers on the arrows represent the mean and the standard error for standardized path coefficients across VI_{sat} datasets ($n = 8$), with blue and red arrows denoting negative and positive effects, respectively. The lower subplots show the direct, intermediary (GUD (A), LAI (B) and TWS (C)) and total effects (TE) of preceding-year precipitation on VI_{sat}.

structural equation models (SEMs), focusing on three mediators: total water storage (TWS, an observational indicator of soil moisture dynamics), leaf area index (LAI) and green-up date (GUD) (Methods).

Increases in preceding-year precipitation enhanced soil moisture, as evidenced by predominantly positive correlations between precipitation and TWS. In regions with positive LPEs, elevated TWS stimulated plant productivity (indicated by VI_{sat}). However, in regions with negative LPEs, TWS had the opposite effect on plant productivity, highlighting the divergent mediating roles of soil moisture in shaping LPE patterns (Fig. 4c). Similarly, preceding-year precipitation showed positive and negative correlations with LAI in areas with positive and negative LPEs, respectively, further exerting contrasting effects on plant productivity (Fig. 4d). Divergent responses of GUD to preceding-year precipitation were also observed, resulting in opposing influences on plant productivity (Fig. 4e). Separate SEM analyses for positive and negative LPEs confirmed distinct pathway effects through the three mediators (Fig. 4f,g). Collectively, these results support all three proposed hypotheses. Besides, we linked preceding-year precipitation to concurrent productivity through intermediate variables generated by GPP models, including LAI, root carbon content, nitrogen uptake and net nitrogen mineralization. These mediating variables effectively captured the spatial patterns of LPEs, exhibiting

predominantly positive effects in regions with positive LPEs and predominantly negative effects in regions with negative LPEs (Supplementary Fig. 20). This suggests that LPEs exert divergent influences on multiple ecophysiological processes associated with productivity.

Discussion

This study provides compelling evidence that preceding-year precipitation exerts a comparable impact on concurrent plant productivity as current-year precipitation, as demonstrated by ground observations and multiple satellite-based metrics (Fig. 1). This lagged response was shaped by climatic context and ecosystem characteristics across site to global scales. Positive LPEs predominate in water-limited regions, whereas negative LPEs are more common in humid areas (Figs. 2 and 3). Notably, the persistence of LPE patterns before and after removing extreme climate events suggests that precipitation memory effects may operate independently of precipitation legacies driven by extremes such as drought (Supplementary Fig. 7). Spatially, aridity emerged as the strongest predictors of LPE variability, underscoring their central roles in governing vegetation–climate interactions. Ground-based analyses revealed predominantly positive LPEs in RWI and ANPP datasets, while GPP_{flux} showed no clear predominance—probably reflecting differences in proxy sensitivity, representativeness or temporal lags in allocation of photosynthate to biomass. Furthermore, regions with higher plant species richness or greater productivity stability were more likely to exhibit weaker or negative LPEs, suggesting that community buffering, trait diversity and resource saturation may dampen productivity responses to prior-year precipitation[35] (Fig. 4a,b and Supplementary Fig. 19).

Mechanistically, LPEs probably arise from the interplay of hydrological memory (snowpack or soil moisture storage), shifts in structural or physiological traits (for example, leaf area, sapwood area, rooting area, tillers and carbon reserves) and climatic controls on growth phenology (Fig. 4). In drylands, our findings align with the 'pulse-reserve' paradigm[36], where antecedent precipitation enhances water and nutrient availability and root development, thereby supporting subsequent productivity. In contrast, in humid systems, negative LPEs may arise from precipitation-regulated soil moisture or cloudiness, leaf development and phenological variations, jointly constraining foliar development and carbon assimilation. In tropical forests specifically, increased precipitation could reduce incoming radiation, lower nutrient cycling rates under increasingly anoxic conditions and limit leaf expansion and photosynthesis despite elevated soil moisture[26,30,31]. Although we highlight LAI as a key structural trait linked to these dynamics, it is best understood as an emergent property of past growth and environmental conditions[33]. Temporal carryover in LAI and phenological shifts probably reflect antecedent physiological processes[37], including carbohydrate storage, hydraulic function, trait plasticity and species-specific leaf turnover—all of which merit further experimental investigation.

Process-based vegetation models partially capture these lagged dynamics. Using LAI, root carbon content, nitrogen uptake and net nitrogen mineralization as intermediate variables, we explored how antecedent precipitation can divergently influence current productivity (Supplementary Fig. 20). Although our carbon-cycle model ensemble—driven by common climate forcing—identified similar aridity-dependent patterns, especially in highlighting tropical forests as negative LPE hotspots, substantial intermodel disagreement points to missing processes (Fig. 3 and Supplementary Fig. 16). These might include incomplete treatment of root turnover, leaf aging, nutrient limitation and carbon allocation memory[5,38,39]. Divergent spatial patterns observed in our results suggest that climatic context, plant traits and soil conditions interact in complex ways that link current productivity with prior precipitation—a coupling rarely addressed in current model frameworks. Thus, our findings highlight the need for in-depth investigations into intermodel discrepancies and enhanced model representations of climatic memory and ecosystem response dynamics to better anticipate shifts in vegetation function and terrestrial carbon cycling under increasing precipitation variability.

Methods

Proxies of plant productivity

Tree-ring width data. We investigated the lagged effect of preceding-year precipitation on tree productivity using chronology-level annual RWI and basal area increment (BAI). RWI was derived from raw tree-ring-width data sourced from the International Tree-Ring Data Bank (ITRDB)[40], applying two detrending methods—spline and modified negative exponential function—to eliminate long-term trends due to aging and increasing trunk diameter[41,42]. From the ITRDB, we analysed 206,765 records across 4,852 sites worldwide spanning 1959–2022, each with ≥20 years of observations. BAI, a two-dimensional metric of wood production[43], was calculated as:

$$\mathrm{BAI} = \pi\left(R_t^2 - R_{t-1}^2\right) \quad (1)$$

where R_t is the tree radius in year t. As field-measured diameters were unavailable in the ITRDB, diameters were estimated by summing annual ring widths, following prior studies[44,45]. Both RWI and BAI were computed using the R package dplR[41]. Primary results were based on spline-derived RWI (Figs. 1 and 2), with consistent findings from modified negative exponential-derived RWI and BAI (Supplementary Fig. 21).

Flux-derived gross primary productivity. We analysed ecosystem-level gross primary productivity (GPP) derived from eddy-covariance flux measurements (GPP_{flux}). After excluding cropland sites and those with <7 yr of data, we retained 68 sites from the FLUXNET2015 database[46], yielding 868 site–year records of annual accumulated GPP.

Grassland aboveground net primary productivity. We compiled long-term ANPP data from two grassland datasets[47,48]. A previous study[47] synthesized ≥10-yr ANPP records from drylands, integrating EcoTrends, Long Term Ecological Research and Oak Ridge National Laboratory Distributed Active Archive Center databases, supplemented by Google Scholar searches for 'aboveground net primary production' or 'ANPP'. Another study[48] aggregated field-based grassland net primary productivity from 438 publications (1957–2018). After excluding time series <7 yr and removing duplicates, we retained 774 site–year records across 50 sites.

Satellite-observed vegetation productivity and growth indices. To examine global LPEs and ensure robustness, we used multiple VI_{sat}. These included four greenness metrics from the moderate resolution imaging spectroradiometer (MODIS) MOD13C2 product[49]—enhanced vegetation index (EVI), normalized difference vegetation index (NDVI) and kernel NDVI—spanning 2001–2022 and NDVI from the global inventory modelling and mapping studies—third generation v.1.2 (GIMMS-3G+) (1982–2022)[50]. We also incorporated two solar-induced chlorophyll fluorescence (SIF) datasets (2001–2022): global OCO-2-based SIF (GOSIF)[51] and continuous solar-induced fluorescence (CSIF)[52], alongside two microwave-based VOD products: Ku-band VOD (1988–2016)[53] and merged-band (C, X, Ku) VOD (1988–2021)[54]. Annual mean indices were used for analysis.

Satellite-derived estimates of GPP. To evaluate GPP_{sat} in capturing LPE, we analysed eight global datasets: global land surface satellite (GLASS) GPP[55], GOSIF-derived GPP[56], multiscale satellite remote sensing (MuSES) GPP[57], MODIS-algorithm GPP[58], two-leaf light use efficiency (TL-LUE) GPP[59], Penman–Monteith–Leuning (PML) v.2 GPP[60], light response function-based (LRF) GPP[61], and machine learning and FLUXNET based carbon and water fluxes (MF-CW) GPP[62]. All datasets

were resampled to 0.5° resolution and annual GPP values were used for analysis.

GPP from dynamic global vegetation models. We assessed the representation of LPE in 18 GPP_{model} from the TRENDY v.11 project[63]: CABLE-POP, CLASSIC, CLM5.0, DLEM, IBIS, ISAM, ISBA-CTRIP, JSBACH, JULES, LPJ-GUESS, LPJ, LPX-Bern, OCN, ORCHIDEE, SDGVM, VISIT, VISIT-NIES and YIBs (Supplementary Table 2). We used the S3 simulation, driven by time-varying forcings (atmosphere CO_2 concentration, climate, land use and nitrogen deposition).

Climate and environmental data

For tree-ring and grassland ANPP analyses, which span the 1950s onward, we used monthly ERA5-Land climate data at 0.1° resolution[64], including precipitation, air temperature, surface downwelling solar radiation and soil moisture (0–100-cm depth). For GPP_{flux} and global-scale gridded analyses (VI_{sat}, GPP_{sat} and GPP_{model}), we used multisource weighted-ensemble precipitation (MSWEP) precipitation[65], multisource weather (MSWX) air temperature and surface downwelling solar radiation[66] and global land evaporation Amsterdam model (GLEAM) root-zone soil moisture[67]. MSWEP integrates gauge-, satellite- and reanalysis-based data, providing reliable global precipitation estimates at 0.1° resolution with daily and monthly temporal resolution from 1979 to near-present[65]. To enhance the robustness of LPE estimates in VI_{sat} analyses, we incorporated additional precipitation datasets: ERA5-Land, Climatic Research Unit (CRU)[68], Climate Prediction Center (CPC)[69] and Global Precipitation Climatology Centre (GPCC)[70]. These precipitation datasets confirmed that preceding-year precipitation has a comparable impact on plant productivity to that of current-year precipitation (Supplementary Fig. 22).

We accounted for atmospheric CO_2 concentration (Ca) and vapour pressure deficit (VPD) in LPE estimates. Ca data were sourced from the NOAA Global Monitoring Laboratory (https://gml.noaa.gov/ccgg/trends/mlo.html). VPD was calculated from monthly air temperature, dewpoint temperature, relative humidity and air pressure data using the R package plantecophys[71], based on ERA5-Land and MSWX data.

Determination of LPEs across scales

To evaluate the influence of past precipitation on plant productivity, we first conducted partial correlation analyses between plant productivity and precipitation at lag 0 (P_t), 1-yr lag (P_{t-1}), 2-yr lag (P_{t-2}) and 3-yr lag (P_{t-3}), while controlling for precipitation during other time periods as well as other climatic variables, including annual mean near-surface temperature (Ta_t) and total surface downwelling solar radiation (Rad_t). Specifically, the partial correlation coefficient between P_{t-1} and current-year productivity (y), $r_{y,P_{t-1}|P_t,P_{t-2},P_{t-3},Ta_t,Rad_t}$, was calculated as:

$$r_{y,P_{t-1}|P_t,P_{t-2},P_{t-3},Ta_t,Rad_t} = \mathrm{corr}(\varepsilon_{y|Z}, \varepsilon_{P_{t-1}|Z}) \quad (2)$$

where $Z = \{P_t, P_{t-2}, P_{t-3}, Ta_t, Rad_t\}$ represents the set of control variables and the terms $\varepsilon_{y|Z}$ and $\varepsilon_{P_{t-1}|Z}$ are the residuals from linear regressions of y and P_{t-1}, respectively, on the control variables Z. This formulation allows us to isolate the unique influence of P_{t-1} while removing the confounding effects of other climate factors. Tree-ring and remote sensing observational data were used in these analyses because of their extensive spatial coverage and long-term records. We then compared the frequencies of sites or grid cells exhibiting significant partial correlations across different lag periods. To further interpret these patterns, sites or grids with significant partial correlations were categorized into four response types: (1) wet_increase—wet years followed by productivity increase (positive correlation); (2) dry_decline—dry years followed by productivity decline (positive correlation); (3) wet_decline—wet years followed by productivity decline (negative correlation); and (4) dry_increase—dry years followed by productivity increase (negative correlation). Wet/dry years and increase/decline in productivity were defined on the basis of annual anomalies of precipitation and productivity proxies (Fig. 1a), with an alternative ±1 s.d. threshold also tested (Supplementary Fig. 23). Before conducting partial correlation analysis, we removed the linear trends of plant productivity and climate variables to better isolate interannual variability.

To further quantify the LPE with 1-yr lag (P_{t-1}), we applied ridge regression using the R package ridge[72]. Ridge regression incorporates an adaptive penalty parameter to mitigate multicollinearity among predictors, reducing the variance of regression coefficients and providing more stable estimates than ordinary least squares[73]. Predictors included P_{t-1} and current-year climate variables (P_t, temperature, radiation, soil moisture, VPD and Ca). Before conducting ridge regression, all variables were detrended and standardized as z-scores[74]. The regression coefficient for P_{t-1} was interpreted as the lagged effect of preceding-year precipitation. We compared absolute ridge-regression sensitivities of P_{t-1} and P_t in regions where either predictor was significant ($P < 0.05$), using this as an indicator of precipitation signal strength[74] (Fig. 1b). Hierarchical partitioning method was used to attribute explained variance to P_{t-1} and P_t (ref. 75). The aridity index, defined as the ratio of precipitation to potential evapotranspiration[76], was used to examine the spatial pattern of LPEs across gradients from drylands to humid regions.

Robustness test for estimating LPEs

To validate calendar-year analyses, we conducted additional test using growing-season data, defined as year-round for the tropics (23° S–23° N), April–October for the extratropical Northern Hemisphere (23° N–90° N) and October–April for the extratropical Southern Hemisphere (23° S–90° S), following previous studies[77,78]. We also estimated LPEs at the biome level using spatial biome patterns from the Ecoregions 2017 dataset[79]. Besides, we assessed the effects of P_{t-1} and P_t on plant productivity after excluding wet and dry years—defined using ±1, ±1.5 and ±2 s.d. thresholds—to examine the influence of climate extremes on LPEs. Beyond partial correlation and ridge regression, we used a nonlinear approach—GAMs—to further evaluate the roles of P_{t-1} and P_t in controlling plant productivity[80]. GAMs were implemented using the R package mgcv[80], with hierarchical partitioning via the package gam.ph quantifying variance explained by P_{t-1} and P_t (ref. 81). Lastly, we incorporated the SPEI[82], as an alternative water availability metric for precipitation, to strengthen analyses of LPE.

To examine whether the LPE is influenced by temporal autocorrelation of precipitation, we analysed the spatial relationship between LPE and 1-yr lag precipitation autocorrelation using both site-level and satellite-derived data. Temporal autocorrelation was calculated with the R package tseries[83]. We found no clear tendency of spatial pattern, as indicated by weak or neutral correlations (Supplementary Figs. 24 and 25). This result supports the robustness of LPE estimation, independent of current-year precipitation, and suggests that LPE is not confounded by temporal autocorrelation in precipitation.

The asymmetric (nonlinear) response of plant productivity to interannual precipitation variability has been proposed as a partial driver of interannual productivity variance[6,32]. To test whether LPE reflects or is influenced by such asymmetry, we also examined the spatial association between LPE and asymmetric responses at both site and global scales. Overall, we observed no dominant spatial relationship (Supplementary Figs. 26 and 27), suggesting that LPE is relatively independent with nonlinear precipitation response. To quantify this asymmetry, we derived an asymmetry index (ASY) to represent the asymmetric response to precipitation based on the log-transformed response ratio (RR) of plant productivity proxies[84,85], calculated as:

$$RR = \ln(PP_i / PP_{base}) \quad (3)$$

where PP_i is the plant productivity in the ith year; PP_{base} is the mean annual plant productivity. Sensitivity of PP to percentage changes in precipitation (St) was computed as:

$$St = RR/\Delta P \quad (4)$$

where ΔP is the percentage deviation from mean annual precipitation. The asymmetry index was defined as:

$$ASY = \overline{St_{wet}} - \overline{St_{dry}} \quad (5)$$

where $\overline{St_{wet}}$ and $\overline{St_{dry}}$ are the absolute value of the mean sensitivity in wet and dry years (precipitation >1 s.d. above or below the mean, respectively). Years with $\Delta P < 1\%$ were excluded to reduce bias from minor precipitation anomalies.

Spatial attribution analysis of LPEs

To identify the primary drivers of the spatial distribution of LPEs, we applied an explainable machine learning approach integrating the SHAP method, using results from tree-ring and VI_{sat} analyses. The response variables were the sensitivity of plant productivity proxies to preceding-year precipitation. The predictors include multiple environmental and biotic factors, which can be classified into three categories: (1) climate factors, encompassing aridity index[76], ERA5-Land snowmelt and the mean values and trends of temperature, precipitation and shortwave radiation; (2) soil factors, comprising soil pH, clay content, nitrogen content, organic carbon content (SoilGrids v.2; ref. 86) and phosphorus content[87]; and (3) biotic factors including plant root depth[88], plant species richness[89], coefficient of variation of vegetation productivity, forest age[90] and tree density[91]—the last two exclusive to the tree-ring analysis. Elevation[92] was also included as a variable. Variable details are provided in Supplementary Table 1.

We built RF models with these factors as predictors and ridge-regression-derived LPE ($P < 0.05$) as the target variable. RF is a data-driven machine learning algorithm well-suited for analysing large datasets, as it can effectively handle complex relationships without imposing statistical assumptions on predictors or target variables[93]. To interpret the RF outcome, we applied SHAP to quantify each predictor marginal contribution to LPE, ranking variable importance by absolute mean SHAP values (absolute weighted average of marginal contributions)[94]. RF models were implemented using the R ranger package[95], with SHAP values extracted via the treeshap package[96].

We further compared ecosystem stability and soil nutrients between ecosystems with positive and negative LPEs from a spatial view. Plant species richness and temporal coefficient of variation of productivity served as indicators of ecosystem stability.

Mediating factors linking preceding-year precipitation to plant productivity

To examine mediators linking preceding-year precipitation to plant productivity, we conducted grid-level partial correlation analyses ($P < 0.05$) using the ensemble of VI_{sat}, evaluating the roles of GUD, LAI[97] and TWS (an observational proxy of soil moisture)[98], while controlling for climatic influences. GUD was estimated as the mean of two methods—dynamic-threshold approach[99] and double-logistic function[100,101]—using GIMMS-3G+ NDVI to minimize methodological uncertainty. SEM was used to quantify direct and indirect pathways between preceding-year precipitation and VI_{sat}, incorporating GUD, LAI and TWS as intermediaries. Grids were classified into two groups based on ridge-regression-derived LPEs: (1) those with significantly positive LPEs and (2) those with significantly negative LPEs ($P < 0.05$). For each group, we assessed three pathways—growing-season extension (via GUD), foliar expansion (via LAI) and enhanced water dynamics (via TWS)—linking preceding-year precipitation to VI_{sat}. All variables were standardized and path coefficients were estimated via maximum-likelihood estimation using the R package lavaan[102]. Path effects were calculated as products of standardized coefficients along each pathway, with total effects derived by summing all relevant path contributions. Model fit was validated using a χ^2-test ($P > 0.05$) and comparative fit index (>0.9), requiring both criteria for acceptance. Ensemble means from partial correlation and SEM analyses across eight VI_{sat} products are reported. In addition, we investigated potential mechanisms by using partial correlation analyses within dynamic global vegetation models, incorporating key vegetation productivity-related variables such as LAI, carbon in roots, nitrogen uptake and net nitrogen mineralization. These model output variables allowed us to assess how vegetation functional traits and belowground dynamics mediate ecosystem responses to preceding-year precipitation.

Reporting summary

Further information on research design is available in the Nature Portfolio Reporting Summary linked to this article.

Data availability

All data used in this study are freely available from the following sources: in situ raw tree-ring-width data are sourced from ITRDB (https://www1.ncdc.noaa.gov/pub/data/paleo/treering/measurements). FLUXNET2015 GPP is available from https://fluxnet.org/data/fluxnet2015-dataset. Grassland ANPP is available via Figshare at https://doi.org/10.6084/m9.figshare.13020695.v1 (ref. 103) and https://doi.org/10.5061/dryad.7sqv9s4vv (ref. 104). MODIS EVI and NDVI are available from https://lpdaac.usgs.gov/products/mod13c2v061/. GOSIF SIF is available from https://data.globalecology.unh.edu/data/GOSIF_v2. CSIF SIF is available from https://doi.org/10.11888/Ecolo.tpdc.271751. Ku VOD is available via Zenodo at https://zenodo.org/records/2575599#.Y5nMg3ZBz9A (ref. 105). Merged-band (C, X, Ku) VOD is available from https://doi.org/10.48436/t74ty-tcx62 (ref. 106). GLASS GPP is available from http://www.glass.umd.edu/Download.html. GOSIF GPP is available from https://data.globalecology.unh.edu/data/GOSIF-GPP_v2. MUSES GPP is available from https://zenodo.org/records/3996814 (ref. 107). MODIS-algorithm GPP is available from https://doi.org/10.1038/nclimate2879. TL-LUE GPP is available via Dryad at https://doi.org/10.5061/dryad.dfn2z352k (ref. 108). PML GPP is available via Figshare at https://doi.org/10.6084/m9.figshare.14185739.v4 (ref. 60). LRF GPP is available from https://doi.org/10.17894/ucph.b2d7ebfb-c69c-4c97-bee7-562edde5ce66. MF-CW GPP is available from https://globalecology.unh.edu/data/MF-CW.html. ERA5-Land data are available from https://doi.org/10.24381/cds.e2161bac. MSWX climate data are available from https://www.gloh2o.org/mswx. MSWEP precipitation is available from https://www.gloh2o.org/mswep. CRU precipitation available from https://data.ceda.ac.uk/badc/cru/data/cru_ts/cru_ts_4.08/data. CPC precipitation is available from https://psl.noaa.gov/data/gridded/data.cpc.globalprecip.html. GPCC precipitation is available from https://doi.org/10.5676/DWD_GPCC/FD_M_V2022_050. Aridity index is available via Figshare at https://doi.org/10.6084/m9.figshare.7504448.v5 (ref. 109). GLEAM soil moisture is available from https://www.gleam.eu. Atmospheric CO_2 concentration is available from https://gml.noaa.gov/ccgg/trends. Terrestrial water storage is available via Figshare at https://doi.org/10.6084/m9.figshare.7670849 (ref. 110). SoilGrids data are available from https://www.isric.org/explore/soilgrids. Soil phosphorus concentration is available via Figshare at https://doi.org/10.6084/m9.figshare.14241854 (ref. 111). GTOPO30 elevation is available from https://doi.org/10.5066/F7DF6PQS. GIMMS LAI 4 g is available via Zenodo at https://doi.org/10.5281/zenodo.7649107 (ref. 112). Plant species richness is available from https://doi.org/10.7910/DVN/PDNWKL. Maximum root depth is available from https://doi.org/10.1073/pnas.1712381114. Forest age is available from https://doi.org/10.17871/ForestAgeBGI.2021. Tree density is available from https://elischolar.library.yale.edu/yale_fes_data/1/. Biome type is available

from https://ecoregions.appspot.com. The field RWI, BAI and related climate data are also available via Zenodo at https://doi.org/10.5281/zenodo.15313896 (ref. 113). Source data are provided with this paper.

Code availability

All data analyses were performed using R (v.4.4.2). The code is available via Zenodo at https://doi.org/10.5281/zenodo.15313896 (ref. 113).

References

1. Huxman, T. E. et al. Convergence across biomes to a common rain-use efficiency. *Nature* **429**, 651–654 (2004).
2. Gherardi, L. A. & Sala, O. E. Enhanced precipitation variability decreases grass- and increases shrub-productivity. *Proc. Natl Acad. Sci. USA* **112**, 12735–12740 (2015).
3. Parton, W. et al. Impact of precipitation dynamics on net ecosystem productivity. *Glob. Change Biol.* **18**, 915–927 (2012).
4. Green, J. K. et al. Large influence of soil moisture on long-term terrestrial carbon uptake. *Nature* **565**, 476–479 (2019).
5. Anderegg, W. R. L. et al. Pervasive drought legacies in forest ecosystems and their implications for carbon cycle models. *Science* **349**, 528–532 (2015).
6. Knapp, A. K., Ciais, P. & Smith, M. D. Reconciling inconsistencies in precipitation–productivity relationships: implications for climate change. *New Phytol.* **214**, 41–47 (2017).
7. Dudney, J. et al. Lagging behind: have we overlooked previous-year rainfall effects in annual grasslands? *J. Ecol.* **105**, 484–495 (2017).
8. Peltier, D. M. P., Anderegg, W. R. L., Guo, J. S. & Ogle, K. Contemporary tree growth shows altered climate memory. *Ecol. Lett.* **25**, 2663–2674 (2022).
9. Sala, O. E., Gherardi, L. A., Reichmann, L., Jobbágy, E. & Peters, D. Legacies of precipitation fluctuations on primary production: theory and data synthesis. *Philos. Trans. R. Soc. B* **367**, 3135–3144 (2012).
10. IPCC *Climate Change 2023: Synthesis Report* (eds Core Writing Team, Lee, H. & Romero, J.) (IPCC, 2023).
11. Zhang, W. et al. Increasing precipitation variability on daily-to-multiyear time scales in a warmer world. *Sci. Adv.* **7**, eabf8021 (2021).
12. Tubiello, F. N., Soussana, J.-F. & Howden, S. M. Crop and pasture response to climate change. *Proc. Natl Acad. Sci. USA* **104**, 19686–19690 (2007).
13. Sloat, L. L. et al. Increasing importance of precipitation variability on global livestock grazing lands. *Nat. Clim. Change* **8**, 214–218 (2018).
14. Reichmann, L. G., Sala, O. E. & Peters, D. P. C. Precipitation legacies in desert grassland primary production occur through previous-year tiller density. *Ecology* **94**, 435–443 (2013).
15. Sun, J. et al. Positive legacies of severe droughts in the Inner Mongolia grassland. *Sci. Adv.* **8**, eadd6249 (2022).
16. Kannenberg, S. A., Schwalm, C. R. & Anderegg, W. R. L. Ghosts of the past: how drought legacy effects shape forest functioning and carbon cycling. *Ecol. Lett.* **23**, 891–901 (2020).
17. Peltier, D. M. P. & Ogle, K. Still recovering or just remembering? To understand drought legacies, modelling choices matter. *J. Ecol.* **111**, 1170–1173 (2023).
18. Müller, L. M. & Bahn, M. Drought legacies and ecosystem responses to subsequent drought. *Glob. Change Biol.* **28**, 5086–5103 (2022).
19. Ogle, K. et al. Quantifying ecological memory in plant and ecosystem processes. *Ecol. Lett.* **18**, 221–235 (2015).
20. Estiarte, M. et al. Few multiyear precipitation–reduction experiments find a shift in the productivity–precipitation relationship. *Glob. Change Biol.* **22**, 2570–2581 (2016).
21. Bazzaz, F. A., Chiariello, N. R., Coley, P. D. & Pitelka, L. F. Allocating resources to reproduction and defense. *BioScience* **37**, 58–67 (1987).
22. Villar-Salvador, P., Uscola, M. & Jacobs, D. F. The role of stored carbohydrates and nitrogen in the growth and stress tolerance of planted forest trees. *New For.* **46**, 813–839 (2015).
23. Sherry, R. A. et al. Lagged effects of experimental warming and doubled precipitation on annual and seasonal aboveground biomass production in a tallgrass prairie. *Glob. Change Biol.* **14**, 2923–2936 (2008).
24. He, L., Li, Z.-L., Wang, X., Xie, Y. & Ye, J.-S. Lagged precipitation effect on plant productivity is influenced collectively by climate and edaphic factors in drylands. *Sci. Total Environ.* **755**, 142506 (2021).
25. Peltier, D. M. P., Barber, J. J. & Ogle, K. Quantifying antecedent climatic drivers of tree growth in the southwestern US. *J. Ecol.* **106**, 613–624 (2018).
26. Schuur, E. A. G. Productivity and global climate revisited: the sensitivity of tropical forest growth to precipitation. *Ecology* **84**, 1165–1170 (2003).
27. Parent, C., Capelli, N., Berger, A., Crèvecoeur, M. & Dat, J. F. An overview of plant responses to soil waterlogging. *Plant Stress* **2**, 20–27 (2008).
28. Zhang, Y., Chen, X., Geng, S. & Zhang, X. A review of soil waterlogging impacts, mechanisms, and adaptive strategies. *Front. Plant Sci.* **16**, 1545912 (2025).
29. Cleveland, C. C. et al. Relationships among net primary productivity, nutrients and climate in tropical rain forest: a pan-tropical analysis. *Ecol. Lett.* **14**, 939–947 (2011).
30. Huete, A. R. et al. Amazon rainforests green-up with sunlight in dry season. *Geophys. Res. Lett.* **33**, 2005GL025583 (2006).
31. Saleska, S. R., Didan, K., Huete, A. R. & Da Rocha, H. R. Amazon forests green-up during 2005 drought. *Science* **318**, 612 (2007).
32. Gherardi, L. A. & Sala, O. E. Effect of interannual precipitation variability on dryland productivity: a global synthesis. *Glob. Change Biol.* **25**, 269–276 (2019).
33. Zhou, B. et al. A general model for the seasonal to decadal dynamics of leaf area. *Glob. Change Biol.* **31**, e70125 (2025).
34. Shen, M., Piao, S., Cong, N., Zhang, G. & Jassens, I. A. Precipitation impacts on vegetation spring phenology on the Tibetan Plateau. *Glob. Change Biol.* **21**, 3647–3656 (2015).
35. Grossiord, C. Having the right neighbors: how tree species diversity modulates drought impacts on forests. *New Phytol.* **228**, 42–49 (2020).
36. Noy-Meir, I. Desert ecosystems: environment and producers. *Annu. Rev. Ecol. Syst.* **4**, 25–51 (1973).
37. Sumida, A., Watanabe, T. & Miyaura, T. Interannual variability of leaf area index of an evergreen conifer stand was affected by carry-over effects from recent climate conditions. *Sci. Rep.* **8**, 13590 (2018).
38. Kolus, H. R. et al. Land carbon models underestimate the severity and duration of drought's impact on plant productivity. *Sci. Rep.* **9**, 2758 (2019).
39. Klesse, S. et al. A combined tree ring and vegetation model assessment of European forest growth sensitivity to interannual climate variability. *Glob. Biogeochem. Cycles* **32**, 1226–1240 (2018).
40. Zhao, S. et al. The International Tree-Ring Data Bank (ITRDB) revisited: data availability and global ecological representativity. *J. Biogeogr.* **46**, 355–368 (2019).
41. Bunn, A. G. A dendrochronology program library in R (dplR). *Dendrochronologia* **26**, 115–124 (2008).
42. Fritts, H. C. & Swetnam, T. W. Dendroecology: a tool for evaluating variations in past and present forest environments. *Adv. Ecol. Res.* **19**, 111–188 (1989).

43. Biondi, F. & Qeadan, F. A theory-driven approach to tree-ring standardization: defining the biological trend from expected basal area increment. *Tree Ring Res.* **64**, 81–96 (2008).
44. Gea-Izquierdo, G. et al. Risky future for Mediterranean forests unless they undergo extreme carbon fertilization. *Glob. Change Biol.* **23**, 2915–2927 (2017).
45. Tao, W. et al. Daytime warming triggers tree growth decline in the Northern Hemisphere. *Glob. Change Biol.* **28**, 4832–4844 (2022).
46. Pastorello, G. et al. The FLUXNET2015 dataset and the ONEFlux processing pipeline for eddy covariance data. *Sci. Data* **7**, 225 (2020).
47. Hou, E. et al. Divergent responses of primary production to increasing precipitation variability in global drylands. *Glob. Change Biol.* **27**, 5225–5237 (2021).
48. Sun, Y., Chang, J. & Fang, J. Above- and belowground net-primary productivity: a field-based global database of grasslands. *Ecology* **104**, e3904 (2023).
49. Didan, K. *MODIS/Terra Vegetation Indices Monthly L3 Global 0.05 Deg CMG V061* [Dataset] (NASA Land Processes DACC, 2021); https://doi.org/10.5067/MODIS/MOD13C2.061
50. Pinzon, J. E. et al. *Vegetation CollectionGlobal Vegetation Greenness (NDVI) from AVHRR GIMMS-3G+, 1981–2022* (ORNL DAAC, 2023); https://doi.org/10.3334/ORNLDAAC/2187
51. Li, X. & Xiao, J. A global, 0.05-degree product of solar-induced chlorophyll fluorescence derived from OCO-2, MODIS, and reanalysis data. *Remote Sens.* **11**, 517 (2019).
52. Zhang, Y., Joiner, J., Alemohammad, S. H., Zhou, S. & Gentine, P. A global spatially contiguous solar-induced fluorescence (CSIF) dataset using neural networks. *Biogeosciences* **15**, 5779–5800 (2018).
53. Moesinger, L. et al. The global long-term microwave Vegetation Optical Depth Climate Archive (VODCA). *Earth Syst. Sci. Data* **12**, 177–196 (2020).
54. Zotta, R.-M. et al. VODCA v2: multi-sensor, multi-frequency vegetation optical depth data for long-term canopy dynamics and biomass monitoring. *Earth Syst. Sci. Data* **16**, 4573–4617 (2024).
55. Liang, S. et al. The global land surface satellite (GLASS) product suite. *Bull. Am. Meteorol. Soc.* **102**, E323–E337 (2021).
56. Li, X. & Xiao, J. Mapping photosynthesis solely from solar-induced chlorophyll fluorescence: a global, fine-resolution dataset of gross primary production derived from OCO-2. *Remote Sens.* **11**, 2563 (2019).
57. Sun, R. et al. Estimation of global net primary productivity from 1981 to 2018 with remote sensing data. In *IGARSS 2020–2020 IEEE International Geoscience and Remote Sensing Symposium* 4331–4334 (IEEE, 2020); https://doi.org/10.1109/IGARSS39084.2020.9323555
58. Kolby Smith, W. et al. Large divergence of satellite and Earth system model estimates of global terrestrial CO_2 fertilization. *Nat. Clim. Change* **6**, 306–310 (2016).
59. Bi, W. et al. A global 0.05° dataset for gross primary production of sunlit and shaded vegetation canopies from 1992 to 2020. *Sci. Data* **9**, 213 (2022).
60. Zhang, X., Zhang, Y. & Kong, D. Global GPP, ET, Ec, Es and Ei simulated by PML-V2 with AVHRR GIMMS3g LAI at a 0.05 degree resolution over 1982–2014. *Figshare* https://doi.org/10.6084/M9.figshare.14185739.V4 (2022).
61. Tagesson, T. et al. A physiology-based Earth observation model indicates stagnation in the global gross primary production during recent decades. *Glob. Change Biol.* **27**, 836–854 (2021).
62. Li, F. et al. Global water use efficiency saturation due to increased vapor pressure deficit. *Science* **381**, 672–677 (2023).
63. Friedlingstein, P. et al. Global carbon budget 2022. *Earth Syst. Sci. Data* **14**, 4811–4900 (2022).
64. Muñoz-Sabater, J. et al. ERA5-Land: a state-of-the-art global reanalysis dataset for land applications. *Earth Syst. Sci. Data* **13**, 4349–4383 (2021).
65. Beck, H. E. et al. MSWEP V2 global 3-hourly 0.1° precipitation: methodology and quantitative assessment. *Bull. Am. Meteorol. Soc.* **100**, 473–500 (2019).
66. Beck, H. E. et al. MSWX: global 3-hourly 0.1° bias-corrected meteorological data including near-real-time updates and forecast ensembles. *Bull. Am. Meteorol. Soc.* **103**, E710–E732 (2022).
67. Martens, B. et al. GLEAM v3: satellite-based land evaporation and root-zone soil moisture. *Geosci. Model Dev.* **10**, 1903–1925 (2017).
68. Harris, I., Osborn, T. J., Jones, P. & Lister, D. Version 4 of the CRU TS monthly high-resolution gridded multivariate climate dataset. *Sci. Data* **7**, 109 (2020).
69. Xie, P. et al. A gauge-based analysis of daily precipitation over East Asia. *J. Hydrometeorol.* **8**, 607–626 (2007).
70. Becker, A. et al. A description of the global land-surface precipitation data products of the Global Precipitation Climatology Centre with sample applications including centennial (trend) analysis from 1901–present. *Earth Syst. Sci. Data* **5**, 71–99 (2013).
71. Duursma, R. A. Plantecophys—an R package for analysing and modelling leaf gas exchange data. *PLoS ONE* **10**, e0143346 (2015).
72. Cule, E. & De Iorio, M. Ridge regression in prediction problems: automatic choice of the ridge parameter. *Genet. Epidemiol.* **37**, 704–714 (2013).
73. Hoerl, A. E. & Kennard, R. W. Ridge regression: biased estimation for nonorthogonal problems. *Technometrics* **12**, 55–67 (1970).
74. Chen, L. et al. Leaf senescence exhibits stronger climatic responses during warm than during cold autumns. *Nat. Clim. Change* **10**, 777–780 (2020).
75. Chevan, A. & Sutherland, M. Hierarchical partitioning. *Am. Stat.* **45**, 90–96 (1991).
76. Zomer, R. J., Xu, J. & Trabucco, A. Version 3 of the global aridity index and potential evapotranspiration database. *Sci. Data* **9**, 409 (2022).
77. Wu, X. et al. Differentiating drought legacy effects on vegetation growth over the temperate Northern Hemisphere. *Glob. Change Biol.* **24**, 504–516 (2018).
78. Jiang, P. et al. Enhanced growth after extreme wetness compensates for post-drought carbon loss in dry forests. *Nat. Commun.* **10**, 195 (2019).
79. Dinerstein, E. et al. An ecoregion-based approach to protecting half the terrestrial realm. *BioScience* **67**, 534–545 (2017).
80. Wood, S. N. *Generalized Additive Models: An Introduction with R* (Chapman and Hall/CRC, 2017).
81. Lai, J., Tang, J., Li, T., Zhang, A. & Mao, L. Evaluating the relative importance of predictors in generalized additive models using the gam.hp R package. *Plant Divers.* **46**, 542–546 (2024).
82. Vicente-Serrano, S. M., Beguería, S. & López-Moreno, J. I. A multiscalar drought index sensitive to global warming: the standardized precipitation evapotranspiration index. *J. Clim.* **23**, 1696–1718 (2010).
83. Trapletti, A. & Hornik, K. tseries: time series analysis and computational finance. R package version 0.10-58 https://doi.org/10.32614/CRAN.package.tseries (1999).
84. Wu, D. et al. Asymmetric responses of primary productivity to altered precipitation simulated by ecosystem models across three long-term grassland sites. *Biogeosciences* **15**, 3421–3437 (2018).

85. Wang, Y., Xiao, J., Li, X. & Niu, S. Global evidence on the asymmetric response of gross primary productivity to interannual precipitation changes. *Sci. Total Environ.* **814**, 152786 (2022).
86. Hengl, T. et al. SoilGrids250m: global gridded soil information based on machine learning. *PLoS ONE* **12**, e0169748 (2017).
87. McDowell, R. W., Noble, A., Pletnyakov, P. & Haygarth, P. M. A global database of soil plant available phosphorus. *Sci. Data* **10**, 125 (2023).
88. Fan, Y., Miguez-Macho, G., Jobbágy, E. G., Jackson, R. B. & Otero-Casal, C. Hydrologic regulation of plant rooting depth. *Proc. Natl Acad. Sci. USA* **114**, 10572–10577 (2017).
89. Ellis, E. C., Antill, E. C. & Kreft, H. All is not loss: plant biodiversity in the anthropocene. *PLoS ONE* **7**, e30535 (2012).
90. Besnard, S. et al. Mapping global forest age from forest inventories, biomass and climate data. *Earth Syst. Sci. Data* **13**, 4881–4896 (2021).
91. Crowther, T. W. et al. Mapping tree density at a global scale. *Nature* **525**, 201–205 (2015).
92. *Global 30 Arc-Second Elevation (GTOPO30)* (EROS USGS, 2017); https://doi.org/10.5066/F7DF6PQS
93. Breiman, L. Random forests. *Mach. Learn.* **45**, 5–32 (2001).
94. Berdugo, M., Gaitán, J. J., Delgado-Baquerizo, M., Crowther, T. W. & Dakos, V. Prevalence and drivers of abrupt vegetation shifts in global drylands. *Proc. Natl Acad. Sci. USA* **119**, e2123393119 (2022).
95. Wright, M. N. & Ziegler, A. ranger: a fast implementation of random forests for high dimensional data in C++ and R. *J. Stat. Soft.* **77**, 1–17 (2017).
96. Lundberg, S. M. et al. From local explanations to global understanding with explainable AI for trees. *Nat. Mach. Intell.* **2**, 56–67 (2020).
97. Cao, S. et al. Spatiotemporally consistent global dataset of the GIMMS leaf area index (GIMMS LAI4g) from 1982 to 2020. *Earth Syst. Sci. Data* **15**, 4877–4899 (2023).
98. Humphrey, V. & Gudmundsson, L. GRACE-REC: a reconstruction of climate-driven water storage changes over the last century. *Earth Syst. Sci. Data* **11**, 1153–1170 (2019).
99. White, M. A., Thornton, P. E. & Running, S. W. A continental phenology model for monitoring vegetation responses to interannual climatic variability. *Glob. Biogeochem. Cycles* **11**, 217–234 (1997).
100. Zhang, X. et al. Monitoring vegetation phenology using MODIS. *Remote Sens. Environ.* **84**, 471–475 (2003).
101. He, L. et al. Non-symmetric responses of leaf onset date to natural warming and cooling in northern ecosystems. *PNAS Nexus* **2**, pgad308 (2023).
102. Rosseel, Y. lavaan: an R package for structural equation modeling. *J. Stat. Soft.* **48**, 1–36 (2012).
103. Hou, E. et al. The effect of interannual precipitation variability on aboveground net primary production [Dataset]. *Figshare* https://doi.org/10.6084/m9.figshare.13020695.v1 (2021).
104. Sun, Y., Chang, J. & Fang, J. Above- and below-ground net primary productivity: a field-based global database of grasslands [Dataset]. *Dryad* https://doi.org/10.5061/dryad.7sqv9s4vv (2022).
105. Moesinger, L. et al. The global long-term microwave vegetation optical depth climate archive VODCA (1.0) [Dataset]. *Zenodo* https://doi.org/10.5281/zenodo.2575599 (2019).
106. Zotta, R.-M. et al. VODCA v2: multi-sensor, multi-frequency vegetation optical depth data for long-term canopy dynamics and biomass monitoring (1.0.0) [Dataset]. *TU Wien* https://doi.org/10.48436/t74ty-tcx62 (2024).
107. Sun, R. et al. Global vegetation productivity from 1981 to 2018 estimated from remote sensing data [Data set]. *Zenodo* https://doi.org/10.5281/zenodo.3996814 (2020).
108. Bi, W. & Zhou, Y. A global 0.05° dataset for gross primary production of sunlit and shaded vegetation canopies (1992–2020) [Dataset]. *Dryad* https://doi.org/10.5061/dryad.dfn2z352k (2022).
109. Zomer, R. J. Global aridity index and potential evapotranspiration (ET0) database: version 3 [Dataset]. *Figshare* https://doi.org/10.6084/m9.figshare.7504448.v5 (2019).
110. Humphrey, V. & Gudmundsson, L. GRACE-REC: a reconstruction of climate-driven water storage changes over the last century [Dataset]. *Figshare* https://doi.org/10.6084/m9.figshare.7670849.v3 (2019).
111. McDowell, R. Global available soil phosphorus database [Dataset]. *Figshare* https://doi.org/10.6084/m9.figshare.14241854.v3 (2023).
112. Cao, S. et al. Spatiotemporally consistent global dataset of the GIMMS leaf area index (GIMMS LAI4g) from 1982 to 2020 (V1.2) [Dataset]. *Zenodo* https://doi.org/10.5281/zenodo.8281930 (2023).
113. He, L. code for LPE study (version v2). *Zenodo* https://doi.org/10.5281/zenodo.15313896 (2025).

Acknowledgements

This study was supported by National Natural Science Foundation of China grant no. 41921001. J.W. was funded by the 'Kezhen and Bingwei' Young Scientist Programme of IGSNRR. D.M.P.P was supported by NSF-DEB grant no. 2213599. J.X. was supported by the University of New Hampshire via bridge support and the Iola Hubbard Climate Change Endowment.

Author contributions

J.W., Z.-L.L. and L.H. designed this study. L.H. performed the analyses and visualization. L.H. and J.W. wrote the first draft of the paper. D.M.P.P., F.R. and P.C. substantially revised the paper with intensive suggestions. All authors discussed the results and contributed to the revisions.

Competing interests

The authors declare no competing interests.

Additional information

Supplementary information The online version contains supplementary material available at https://doi.org/10.1038/s41559-025-02806-4.

Correspondence and requests for materials should be addressed to Jian Wang or Zhao-Liang Li.

Peer review information *Nature Ecology & Evolution* thanks the anonymous reviewers for their contribution to the peer review of this work. Peer reviewer reports are available.

[1]State Key Laboratory of Efficient Utilization of Arable Land in China, Institute of Agricultural Resources and Regional Planning, Chinese Academy of Agricultural Sciences, Beijing, China. [2]The Key Laboratory of Land Surface Pattern and Simulation, Institute of Geographical Sciences and Natural Resources Research, Chinese Academy of Sciences, Beijing, China. [3]University of the Chinese Academy of Sciences, Beijing, China. [4]School of Life Sciences, University of Nevada-Las Vegas, Las Vegas, NV, USA. [5]Laboratoire des Sciences du Climat et de l'Environnement, CEA/CNRS/UVSQ/ Université Paris Saclay, Gif-sur-Yvette, France. [6]CSIC, Global Ecology CREAF-CSIC-UAB, Cerdanyola del Vallès, Barcelona, Spain. [7]CREAF, Cerdanyola del Vallès, Barcelona, Spain. [8]Earth Systems Research Center, Institute for the Study of Earth, Oceans, and Space, University of New Hampshire, Durham, NH, USA. [9]Institute of Integrative Biology, ETH Zurich (Swiss Federal Institute of Technology), Zurich, Switzerland. [10]School of Geography and Planning, Sun Yat-sen University, Guangzhou, China. [11]State Key Laboratory of Herbage Improvement and Grassland Agro-Ecosystems, College of Ecology, Lanzhou University, Lanzhou, China. [12]Graduate School of Environment and Information Science, Yokohama National University, Yokohama, Japan. [13]Center for Ocean Remote Sensing of Southern Marine Science and Engineering Guangdong Laboratory (Guangzhou), Guangzhou Institute of Geography, Guangdong Academy of Sciences, Guangzhou, China. [14]State Key Laboratory of Resources and Environmental Information System, Institute of Geographic Sciences and Natural Resources Research, Chinese Academy of Sciences, Beijing, China. ✉e-mail: wangjian@igsnrr.ac.cn; lizhaoliang@caas.cn

nature portfolio

Corresponding author(s): Jian Wang & Zhao-Liang Li

Last updated by author(s): Jun 14, 2025

Reporting Summary

Nature Portfolio wishes to improve the reproducibility of the work that we publish. This form provides structure for consistency and transparency in reporting. For further information on Nature Portfolio policies, see our Editorial Policies and the Editorial Policy Checklist.

Statistics

For all statistical analyses, confirm that the following items are present in the figure legend, table legend, main text, or Methods section.

n/a	Confirmed
☐	☒ The exact sample size (*n*) for each experimental group/condition, given as a discrete number and unit of measurement
☐	☒ A statement on whether measurements were taken from distinct samples or whether the same sample was measured repeatedly
☐	☒ The statistical test(s) used AND whether they are one- or two-sided *Only common tests should be described solely by name; describe more complex techniques in the Methods section.*
☒	☐ A description of all covariates tested
☐	☒ A description of any assumptions or corrections, such as tests of normality and adjustment for multiple comparisons
☐	☒ A full description of the statistical parameters including central tendency (e.g. means) or other basic estimates (e.g. regression coefficient) AND variation (e.g. standard deviation) or associated estimates of uncertainty (e.g. confidence intervals)
☐	☒ For null hypothesis testing, the test statistic (e.g. *F*, *t*, *r*) with confidence intervals, effect sizes, degrees of freedom and *P* value noted *Give P values as exact values whenever suitable.*
☒	☐ For Bayesian analysis, information on the choice of priors and Markov chain Monte Carlo settings
☒	☐ For hierarchical and complex designs, identification of the appropriate level for tests and full reporting of outcomes
☒	☐ Estimates of effect sizes (e.g. Cohen's *d*, Pearson's *r*), indicating how they were calculated

Our web collection on statistics for biologists contains articles on many of the points above.

Software and code

Policy information about availability of computer code

Data collection	No software was used.
Data analysis	R studio (v4.4.2) was used to conduct data preprocessing and all analyses.

For manuscripts utilizing custom algorithms or software that are central to the research but not yet described in published literature, software must be made available to editors and reviewers. We strongly encourage code deposition in a community repository (e.g. GitHub). See the Nature Portfolio guidelines for submitting code & software for further information.

Data

Policy information about availability of data

All manuscripts must include a data availability statement. This statement should provide the following information, where applicable:

- Accession codes, unique identifiers, or web links for publicly available datasets
- A description of any restrictions on data availability
- For clinical datasets or third party data, please ensure that the statement adheres to our policy

Code availability
All data analyses were performed using R (v4.4.2). The code is stored in a publicly available Zenodo repository (https://doi.org/10.5281/zenodo.15313896).

Data availability

All data used in this study are freely available from the following sources: In situ raw tree-ring width data are sourced from the International Tree-Ring Data Bank (ITRDB) (https://www1.ncdc.noaa.gov/pub/data/paleo/treering/measurements). FLUXNET2015 GPP is available from https://fluxnet.org/data/fluxnet2015-dataset. Grassland ANPP is available from https://doi.org/10.6084/m9.figshare.13020695.v1 and https://doi.org/10.5061/dryad.7sqv9s4vv. MODIS EVI and NDVI are available from https://lpdaac.usgs.gov/products/mod13c2v061/. GOSIF SIF is available from https://data.globalecology.unh.edu/data/GOSIF_v2. CSIF SIF is available from https://doi.org/10.11888/Ecolo.tpdc.271751. Ku VOD is available from https://zenodo.org/records/2575599#.Y5nMg3ZBz9A. Merged-band (C, X, Ku) VOD is available from https://doi.org/10.48436/t74ty-tcx62. GLASS GPP is available from http://www.glass.umd.edu/Download.html. GOSIF GPP is available from https://data.globalecology.unh.edu/data/GOSIF-GPP_v2. MUSES GPP is available from https://zenodo.org/records/3996814. MODIS-algorithm GPP is available from https://doi.org/10.1038/nclimate2879. TL-LUE GPP is available from https://doi.org/10.5061/dryad.dfn2z352k. PML GPP is available from https://doi.org/10.6084/m9.figshare.14185739.v4. LRF GPP is available from https://doi.org/10.17894/ucph.b2d7ebfb-c69c-4c97-bee7-562edde5ce66. MF-CW GPP is available from https://globalecology.unh.edu/data/MF-CW.html. ERA5-Land data are available from https://doi.org/10.24381/cds.e2161bac. MSWX climate data are available from https://www.gloh2o.org/mswx. MSWEP precipitation is available from https://www.gloh2o.org/mswep. CRU precipitation available from https://data.ceda.ac.uk/badc/cru/data/cru_ts/cru_ts_4.08/data. CPC precipitation is available from https://psl.noaa.gov/data/gridded/data.cpc.globalprecip.html. GPCC precipitation is available from http://dx.doi.org/10.5676/DWD_GPCC/FD_M_V2022_050. Aridity index is available from https://doi.org/10.6084/m9.figshare.7504448.v5. GLEAM soil moisture is available from https://www.gleam.eu. Atmospheric CO2 concentration is available from https://gml.noaa.gov/ccgg/trends. Terrestrial water storage is available from https://doi.org/10.6084/m9.figshare.7670849. SoilGrids data are available from https://www.isric.org/explore/soilgrids. Soil phosphorus concentration is available from https://doi.org/10.6084/m9.figshare.14241854. GTOPO30 elevation is available from https://doi.org/10.5066/F7DF6PQS. GIMMS LAI 4g is available from https://doi.org/10.5281/zenodo.7649107. Plant species richness is available from https://doi.org/10.7910/DVN/PDNWKL. Maximum root depth is available from https://doi.org/10.1073/pnas.1712381114. Forest age is available from https://doi.org/10.17871/ForestAgeBGI.2021. Tree density is available from https://elischolar.library.yale.edu/yale_fes_data/1/. Biome type is available from https://ecoregions.appspot.com. The field RWI, BAI and related climate data are also stored in a publicly available Zenodo repository (https://doi.org/10.5281/zenodo.15313896). Source data are provided with this paper.

Research involving human participants, their data, or biological material

Policy information about studies with human participants or human data. See also policy information about sex, gender (identity/presentation), and sexual orientation and race, ethnicity and racism.

Reporting on sex and gender	N/A
Reporting on race, ethnicity, or other socially relevant groupings	N/A
Population characteristics	N/A
Recruitment	N/A
Ethics oversight	N/A

Note that full information on the approval of the study protocol must also be provided in the manuscript.

Field-specific reporting

Please select the one below that is the best fit for your research. If you are not sure, read the appropriate sections before making your selection.

☐ Life sciences ☐ Behavioural & social sciences ☒ Ecological, evolutionary & environmental sciences

For a reference copy of the document with all sections, see nature.com/documents/nr-reporting-summary-flat.pdf

Ecological, evolutionary & environmental sciences study design

All studies must disclose on these points even when the disclosure is negative.

Study description	This study focused on the responses of vegetation productivity to preceding precipitation from site to global scales and underlying biogeophysical mechanisms.
Research sample	We used three global-scale networks of ground monitoring representing various plant species and functional types, including records of the tree ring-width index (RWI, a proxy of tree annual growth), eddy-covariance flux measurements of gross primary productivity (GPPflux), and grass aboveground net primary production (ANPP). We also leveraged eight satellite-observed vegetation productivity/growth indicators (VGIsat), eight satellite-derived estimates of GPP (GPPsat), and GPP simulations from 18 carbon-cycle models (GPPmodel) spanning from 1950 to 2022.
Sampling strategy	The analyzed data in our study were obtained from open-access database instead of designed experiments, sampling is not applicable to our study.
Data collection	All data used in this study are available online. The specific links for each dataset are presented in Supplementary Tables 1.
Timing and spatial scale	Between 1950-2022. Terrestrial ecosystems over the world.

Data exclusions	No data was exclude in our analyses.
Reproducibility	The ground- and satellite-based data, and climate data are open access. The findings of our study can be reproduced using the statistical methods shown in the manuscript.
Randomization	The analyzed data in our study were obtained from open-access database instead of designed experiments, randomization is not applicable to our study.
Blinding	The analyzed data in our study were obtained from open-access database instead of designed experiments, blinding is not applicable to our study.

Did the study involve field work? ☐ Yes ☒ No

Reporting for specific materials, systems and methods

We require information from authors about some types of materials, experimental systems and methods used in many studies. Here, indicate whether each material, system or method listed is relevant to your study. If you are not sure if a list item applies to your research, read the appropriate section before selecting a response.

Materials & experimental systems

n/a	Involved in the study
☒	☐ Antibodies
☒	☐ Eukaryotic cell lines
☒	☐ Palaeontology and archaeology
☒	☐ Animals and other organisms
☒	☐ Clinical data
☒	☐ Dual use research of concern
☒	☐ Plants

Methods

n/a	Involved in the study
☒	☐ ChIP-seq
☒	☐ Flow cytometry
☒	☐ MRI-based neuroimaging

Plants

Seed stocks	N/A
Novel plant genotypes	N/A
Authentication	N/A